

Linear and nonlinear stabilities analysis of gaseous detonation waves in complex reactive systems

Junhui Zhang, and Gang Dong*

National Key Laboratory of Transient Physics, Nanjing University of Science and Technology, Nanjing 210094, China

Received October 15, 2024; accepted December 1, 2024; published online March 6, 2025

The stability of gaseous detonation waves is crucial for the operation of detonation-based propulsion systems and the assessment of industrial explosion hazards. However, research on the stability of detonation waves in complex reactive systems that are composed of actual fuels and oxidants and can be described by numerous elementary chemical reactions, has not been fully carried out. To investigate the relationship between linear and nonlinear stabilities in gaseous detonation wave propagation for complex reactive systems, the linear stability analysis and the one-dimensionally nonlinear numerical simulations of $\text{H}_2/\text{O}_2/\text{Ar}$ (argon) detonations based on the reactive Euler equations and detailed reaction mechanisms are carried out. The results show that in complex reactive systems characterized by elementary chemical reactions, the results of linear stability computation of detonation are consistent with those from one-dimensionally nonlinear oscillations of detonation wave. Utilizing these linear stability results, a neutral stability curve and a perturbation frequency transition curve in the phase plane of initial pressure versus inert gas (Ar) dilution ratio are derived, especially the new frequency transition curve clearly describes the transition of perturbations from low-frequency to high-frequency mode. One-dimensional nonlinear simulations show that near the perturbation frequency transition curve, the oscillations of the detonation wave can also transform between the low-frequency, high-amplitude oscillation mode and the high-frequency, low-amplitude oscillation mode, with the oscillation frequency corresponding to the mode that exhibits the maximum growth rate identified in the linear stability analysis. This investigation into detonation stability in complex reactive gases offers guidance for selecting appropriate initial conditions and gas compositions in practical applications of detonation.

Linear stability, Nonlinear stability, Perturbation mode, Detailed reaction mechanism, Gaseous detonation

Citation: J. Zhang, and G. Dong, Linear and nonlinear stabilities analysis of gaseous detonation waves in complex reactive systems, Acta Mech. Sin. 41, 324750 (2025), <https://doi.org/10.1007/s10409-024-24750-x>

1. Introduction

Detonation is an extremely rapid self-sustaining combustion phenomenon. Unlike ordinary combustion, the propagation speed of detonation wave exceeds the sound velocity, resulting in extremely high temperature and pressure. Gaseous detonation phenomena widely exist in fields such as safety assessment [1] and propulsion technology [2]. However, the stability of detonations remains a critical issue in these applications, as unstable detonations can lead to propagation failures of detonation waves or unpredictable hazards. Understanding the underlying mechanisms of these instabilities

and identifying stability criteria are essential for any practical application utilizing detonation waves for rapid energy conversion.

In the 1960s, Erpenbeck [3,4] first theoretically studied the linear stability of detonations. By applying an infinitesimal perturbation to the reactive Euler equations and using Laplace transform to deal with the initial conditions, he obtained a function to determine the stability of one-dimensional detonation. In 1990, Lee and Stewart [5] further innovatively proposed a normal mode method to solve the linear stability problem. The method uses a single-step Arrhenius reaction model and a numerical method based on the shooting algorithm to determine the eigenvalues of linearized equations of the normal perturbations, which satisfy the

*Corresponding author. E-mail address: gdong@njust.edu.cn (Gang Dong)
Executive Editor: Guohua Tu

conditions of the detonation wave at the equilibrium point or the sound velocity point (boundary conditions). This method greatly reduces the complexity of the computation and is currently the main method for computing the linear stability of gaseous detonations.

In practical applications, due to the specific thermodynamic and kinetic characteristics of combustible gases, or wall effects and other factors, the non-ideal detonations often occur. In non-ideal detonations, the sonic plane is located inside the chemical reaction zone, so only the chemical heat release between the leading shock front and the sonic plane can be utilized to support the propagation of the detonation wave, which reduces the stability of the detonation wave. In view of the above phenomena, the stability of non-ideal detonation has been studied by using the normal mode method, including pathological detonation [6] and weak detonation [7]. In addition, linear stabilities considering gas non-equilibrium effect [8] and the molecular effect of detonation [9] have also been carried out. These studies not only extend the range of linear stability theory applications but also provide theoretical support and guidance for practical engineering solutions.

For reaction models applied to detonation linear stability computations, the single-step Arrhenius reaction has been widely used, a significant limitation of the single-step reaction is its inability to replicate the distinct finite regions of the induction and recombination zones within the reaction zone of detonation wave, in which reactants are converted into products through a series of branching chain reactions in practical detonations. Consequently, the normal mode method has also been applied to more realistic reaction models, including two-step consecutive reactions [6,10], three-step chain-branching reactions [11], four-step chain-branching reactions [12] and one-step reversible reactions [13], et al. However, the linear stability of detonation waves in complex reactive systems, involving detailed reaction mechanism composed of elementary reactions, has not been reported yet.

Despite the widespread use of the normal mode method for studying linear stability issues in detonations, challenges remain in accurately handling boundary conditions, particularly radiation conditions at the rear boundary of reaction zone of detonation wave. To address this, Sharpe [10] conducted a complex asymptotic analysis of perturbations near the sonic plane in reaction zone of detonation wave to derive asymptotic analytical boundary conditions for correctly identifying eigenvalues. However, applying these boundary conditions typically constitute the most complex aspect of solving linear stability in the normal mode method. To circumvent this issue, Kabanov and Kasimov [14] developed a novel method for computing the linear stability of detonations without requiring the addition of radiation conditions at the rear boundary. The computation costs are

not significantly increased when more complex chemical reaction models are used, which makes it possible to analyze the linear stability of detonation waves in complex reaction systems, especially for those composed of elementary reactions.

This paper aims to explore the linear stability characteristics of gaseous detonation for $H_2/O_2/Ar$ mixture. The method by Kabanov and Kasimov [14] is employed to resolve the linear stability problem which involves detailed chemical reaction mechanisms in complex reactive systems. The nonlinear stability of one-dimensionally longitudinal oscillation of detonation waves is also studied and compared with the linear one. The effects of initial pressure and dilution ratio of inert gas in the reactive system on both the linear and nonlinear stabilities are focused on. The paper is organized as follows: Sects. 2 and 3 present linear and nonlinear stability methods, respectively. Section 4 analyzes the linear stability spectra of detonations under the conditions of varying initial pressure and dilution ratio of inert gas and compares the linear results with corresponding nonlinear ones. Especially, the critical curves associated with stability criterion in a phase plane are obtained and discussed. Section 5 presents the conclusions.

2. Linear stability analysis method

The fundamental approach to linear stability analysis involves decomposing the physical quantities in the governing equations that describe the propagation of gas-phase detonation waves into mean and perturbation components. By neglecting the influence of higher-order perturbations, the linearized equations for the perturbations can be obtained. Subsequently, appropriate methods are employed to determine the characteristics of perturbation growth (indicating instability) or decay (indicating stability) over time in the linearized equations.

2.1 Governing equation

The governing equations for gaseous detonations used in present study are the one-dimensionally reactive Euler equations

$$\frac{\partial v}{\partial t} + U \frac{\partial v}{\partial X} - v \frac{\partial U}{\partial X} = 0, \quad (1)$$

$$\frac{\partial U}{\partial t} + U \frac{\partial U}{\partial X} + v \frac{\partial p}{\partial X} = 0, \quad (2)$$

$$\frac{\partial e}{\partial t} + p \frac{\partial v}{\partial t} + U \frac{\partial e}{\partial X} + pU \frac{\partial v}{\partial X} = 0, \quad (3)$$

$$\frac{\partial Y_i}{\partial t} + U \frac{\partial Y_i}{\partial X} = \Omega_i, \quad i = 1, \dots, N, \quad (4)$$

where v is the specific volume ($v=1/\rho$, ρ the density); U is the velocity of fluid particles in the laboratory coordinate system (X); p is the pressure; e is the specific internal energy; Y_i is the mass fraction of species i ; Ω_i is the net production rate of species i ; and N represents the number of species contained in the complex reactive system. In order to investigate the influence of the elementary reactions, a detailed chemical reaction mechanism of $H_2/O_2/Ar$ (argon) [15] was adopted in this paper, which includes 9 species and 19 elementary reactions. It is assumed that thermally perfect gas in the reaction system is adopted, the equation of state for ideal gas is then used to describe change of the thermodynamic state in the system.

To facilitate the linearization of the energy equation, original energy equation (Eq. (3)) needs to be expressed as follows, using the form derived by Kao [13]

$$\frac{\partial p}{\partial t} + U \frac{\partial p}{\partial X} + \frac{a_f^2}{v} \frac{\partial u}{\partial X} = Z(v, p, \mathbf{Y}), \quad (5)$$

$$Z(v, p, \mathbf{Y}) = -\frac{G}{v} \sum_{i=1}^N \frac{\partial e}{\partial Y_i} \Big|_{p, v, Y_{j \neq i}} \Omega_i, \quad i = 1, \dots, N, \quad (6)$$

where a_f is the frozen sound speed; G is the Grüneisen

coefficient; $\mathbf{Y}=[Y_1, Y_2, \dots, Y_N]^T$ is the vector of mass fractions of the species (Y_i); and $Z(v, p, \mathbf{Y})$ is determined by the partial derivatives of the specific internal energy with respect to each species.

Using the coordinate attached to shock wave and placing the shock wave at the origin of the coordinate axis, the spatial position x and fluid particle velocity u in the new coordinate system can be expressed as follows:

$$x = X - Dt, \quad u = U - D, \quad (7)$$

where u is the velocity in the shock coordinate system (x); and D is the speed of the detonation wave. In the new coordinate system, the transformation relation for the differential operator is given by

$$\frac{\partial}{\partial X} = \frac{\partial}{\partial x}, \quad \frac{\partial}{\partial t} = \frac{\partial}{\partial t} - D \frac{\partial}{\partial x}. \quad (8)$$

Thus, the governing Eqs. (1), (2), (4), and (5) can be written in the form of the following matrix.

$$\mathbf{z}_{,t} + \mathbf{A} \cdot \mathbf{z}_{,x} = \mathbf{c}, \quad (9)$$

where the subscripts “ t ” and “ x ” represent the partial derivatives with respect to time and spatial distance, respectively; and the matrix \mathbf{z} , \mathbf{c} , and \mathbf{A} can be represented as

$$\mathbf{z} = \begin{pmatrix} v \\ U \\ p \\ Y_1 \\ \vdots \\ Y_N \end{pmatrix}, \quad \mathbf{c} = \begin{pmatrix} 0 \\ 0 \\ Z(v, p, \mathbf{Y}) \\ \Omega_1 \\ \vdots \\ \Omega_N \end{pmatrix}, \quad \mathbf{A} = \begin{pmatrix} U-D & -v & 0 & 0 & \dots & 0 \\ 0 & U-D & 0 & v & \dots & 0 \\ 0 & \rho a_f^2 & U-D & 0 & \dots & 0 \\ 0 & 0 & 0 & U-D & \dots & 0 \\ \vdots & \vdots & \vdots & \vdots & \ddots & \vdots \\ 0 & 0 & 0 & 0 & 0 & U-D \end{pmatrix}. \quad (10)$$

2.2 Perturbation linear equations in the coordinate attached to shock wave

In the present work, a method developed by Kabanov and Kasimov [14] is used to solve the linear stability problem of detonation waves. The method consists of two steps. The first step is to numerically solve the linearized equations of perturbations, in order to obtain the time series of speed perturbations of propagating detonation wave. In the second step, a dynamic mode decomposition (DMD) method [16] is used to process the results from the first step to extract the stability spectra of the perturbation. Unlike the normal mode method, this method does not require any special treatment of the sonic plane within the reaction zone of detonation wave, thus making it easier to extend to more complex chemical reactions and equations of state.

Before proceeding with the computations mentioned above, the form of the linearized governing equation of perturbations should be given first. To achieve this, we can

decompose the quantities to be solved in governing Eq. (9) into steady-state and perturbation components, resulting in the following expression

$$\mathbf{z}(x, t) = \mathbf{z}^*(x) + \varepsilon \mathbf{z}'(x, t), \quad (11)$$

$$D(t) = D^* + \varepsilon \psi'(t), \quad (12)$$

where the superscript “ $*$ ” denotes the steady-state solutions; the superscript “ $'$ ” denotes the perturbation solutions; $\mathbf{z}'=[v', U', p', Y_1', \dots, Y_N']^T$; and ψ' is the speed perturbation of the propagating detonation wave, $0 < \varepsilon \ll 1$.

By introducing Eqs. (11)-(12) into Eq. (9) and omitting the high-order nonlinear term, the following linearized governing equations of perturbations are obtained

$$\mathbf{z}'_{,t} + \mathbf{A}^* \mathbf{z}'_{,x} + \mathbf{B}^* \mathbf{z}' - \mathbf{z}^*_{,x} \psi' = \mathbf{0}, \quad (13)$$

where \mathbf{A}^* denotes the steady-state solution of \mathbf{A} ; and the expression of \mathbf{B}^* is as follows:

$$\mathbf{B}^* = \begin{pmatrix} -U_{,x} & v_{,x} & 0 & 0 & \dots & 0 \\ p_{,x} & U_{,x} & 0 & 0 & \dots & 0 \\ (\rho a_f^2)_{,v} U_{,x} - Z_{,v} & p_{,x} & (\rho a_f^2)_{,p} U_{,x} - Z_{,p} & (\rho a_f^2)_{,Y_1} U_{,x} - Z_{,Y_1} & \dots & (\rho a_f^2)_{,Y_N} U_{,x} - Z_{,Y_N} \\ -\Omega_{1,v} & Y_{1,x} & -\Omega_{1,p} & -\Omega_{1,Y_1} & \dots & -\Omega_{1,Y_N} \\ \vdots & \vdots & \vdots & \vdots & \ddots & \vdots \\ -\Omega_{N,v} & Y_{N,x} & -\Omega_{N,p} & -\Omega_{N,Y_1} & \dots & -\Omega_{N,Y_N} \end{pmatrix}, \quad (14)$$

where the subscripts “ x ”, “ v ” and “ p ” represent the partial derivatives of the variables with respect to spatial distance, specific volume and pressure, while the subscripts “ Y_1 ”, ..., “ Y_N ” represent the derivatives with respect to the mass fraction of species. Note that the Eqs. (13) and (14) are the extension of original perturbation linear equations [14] in complex reactive system with arbitrary number of species, thus those partial derivatives associated with species i ($i=1, \dots, N$), such as, $Z_{,Y_i}$, $Y_{i,x}$, $\Omega_{i,v}$, $\Omega_{i,p}$, Ω_{i,Y_i} , $Z_{,Y_i}$ and $Y_{i,x}$ in matrix \mathbf{B}^* of Eq. (14) and $\partial e/\partial Y_i$ in Eq. (6) are determined or calculated independently in present study.

Since Eq. (13) contains $N+3$ governing equations but has $N+4$ unknowns (ψ' lacks evolution equations), the equations are not closed. Therefore, it is necessary to supplement the evolution equation for ψ' . For this reason, we adopt the equation derived in the Ref. [17]

$$\frac{dD}{dt} = -v_a s, \quad (15)$$

$$s = \frac{1}{A_0}(Z - A_s), \quad A_0 = -\frac{2D}{\gamma_a + 1} \left(3 + \frac{\gamma_a p_a v_a}{D^2} \right),$$

$$A_s = \left. \frac{(a_f^2 - u^2)}{v} U_{,x} \right|_s, \quad (16)$$

where the subscript “ s ” is the state just behind the shock wave; the subscript “ a ” is the state before the shock wave; and γ is the adiabatic index.

Using Eqs. (11) and (12), we linearize the evolution equation for the detonation speed D given by Eq. (15) and obtain the evolution equation for speed perturbation ψ'

$$\frac{d\psi'}{dt} = -v_a s', \quad (17)$$

$$s' = \frac{1}{A_0}(Z'_s - A'_s) - \frac{A'_0}{A_0^2}(Z_s^* - A_s^*), \quad (18)$$

$$A'_0 = \frac{2}{\gamma_a + 1} \frac{\gamma_a p_a v_a - 3D^{*2}}{D^{*2}} \psi', \quad Z'_s = \left[Z_{,p}^* \psi' - \frac{Z_{,v}^*}{v^2} v' \right]_s,$$

$$A'_s = \left\{ \frac{[\gamma_a(pv' + vp') - 2uv']}{v^*} U_{,x}^* - \frac{(a_f^2 - u^2) U_{,x}^*}{v^{*2}} v' + \frac{(a_f^2 - u^2)}{v^*} U_{,x}' \right\}_s. \quad (19)$$

2.3 Boundary conditions and numerical methods

In the previous section, we have linearized the governing equations and obtained the partial differential equations (PDEs) regarding \mathbf{z}' (Eq. (13)) and ψ' (Eq. (17)). To solve the PDEs, we first define the length of the one-dimensional computational domain to be 30 times the induction zone length l_{ind} , ensuring that the reaction zone falls completely within the domain. Here the l_{ind} is defined as the distance from the location of the leading shock front of the detonation wave to the position of maximum heat release rate in the reaction zone. Next, we discretize the computational domain using a uniform grid $\{x_i\}$, $i=0, \dots, M$.

Appropriate boundary conditions are specified at the starting and ending positions of the computational domain. The starting position corresponds to $x_M=0$, while the ending position corresponds to $x_0=-30 l_{\text{ind}}$. At $x_M=0$, the boundary condition just behind the leading shock front of the detonation wave can be described using the Rankine-Hugoniot relations, which provide a conservation relationship for the state variables before and after the shock wave, as follows:

$$p_s = -\frac{\gamma_a - 1}{\gamma_a + 1} p_a + \frac{2}{(\gamma_a + 1)v_a} D^2,$$

$$v_s = \frac{\gamma_a - 1}{\gamma_a + 1} v_a - \frac{2}{\gamma + 1} \frac{\gamma_a p_a v_a^2}{D^2}, \quad (20)$$

$$U_s = D_s, \quad \mathbf{Y}_s = \mathbf{0}.$$

Linearize Eq. (20) to obtain the final form representation at the boundary as follows:

$$p'_s = -\frac{4D^*}{(\gamma_a + 1)v_a} \psi', \quad v'_s = -\frac{4\gamma p_a v_a^2}{(\gamma_a + 1)D^{*3}} \psi',$$

$$U'_s = \frac{D^*}{v_a} v'_s - \psi', \quad \mathbf{Y}'_s = \mathbf{0}. \quad (21)$$

The boundary condition at $x_0 = -30 l_{\text{ind}}$ is set as a zero gradient boundary condition, which avoids the complex radiation boundary conditions used in the normal mode method. Thus, the computation is greatly simplified, which is very favorable for the computation of complex chemical reaction models. We also need to provide initial conditions for \mathbf{z}' and ψ' . Firstly, the initial speed perturbation is specified as $\psi'|_{t=0}=0.01$. The Rankine-Hugoniot conditions are then used to find v'_s , U'_s , and p'_s from ψ' . Subsequently, initial conditions for perturbations over the whole grid are

computed by using

$$\begin{aligned} v'|_{t=0} &= \frac{v'_s}{v_s^*} v^*(x), U'|_{t=0} = \frac{U'_s}{U_s^*} U^*(x), \\ p'|_{t=0} &= \frac{P'_s}{P_s^*} p^*(x), Y'_i|_{t=0} = \frac{Y'_s}{Y_s^*} Y_i^*(x), \quad i = 1, \dots, N, \end{aligned} \quad (22)$$

where $v^*(x)$, $U^*(x)$, $p^*(x)$ and $Y_i^*(x)$ are the steady-state solutions of specific volume, the velocity of fluid particles, pressure, and species, respectively, as functions of x .

The partial derivatives of the thermodynamic parameters and kinetic parameters that appeared in above equations and matrices can be determined by using Cantera [18] and SDtoolbox [19].

Given the boundary conditions of the linearized Eqs. (13) and (17), a finite difference scheme [14] is adopted to approximate the spatial derivatives on each grid point at the current moment, thus the linearized PDEs are transformed into the ordinary differential equations (ODEs) only with respect to time

$$\frac{d\mathbf{z}'_i}{dt} = -\widehat{\mathbf{L}}(\mathbf{z}^*, \mathbf{z}'), \quad i = 1, \dots, M-1, \quad (23)$$

$$\frac{d\psi'}{dt} = -v_a \widehat{s}'(\mathbf{z}^*, \mathbf{z}'), \quad (24)$$

where $\widehat{\mathbf{L}}(\mathbf{z}^*, \mathbf{z}')$ and $\widehat{s}'(\mathbf{z}^*, \mathbf{z}')$ are the numerical approximations of $\mathbf{L}(\mathbf{z}^*, \mathbf{z}', \mathbf{z}'_{,x}) = \mathbf{A}^*(\mathbf{z}^*)\mathbf{z}'_{,x} + \mathbf{B}^*(\mathbf{z}^*)\mathbf{z}' - \mathbf{z}^*_{,x}\psi'$ from Eq. (13) and $s'(\mathbf{z}^*, \mathbf{z}', \mathbf{z}'_{,x})$ from Eq. (17). The time series of ψ' controlled by the linearized equation can be obtained by integrating the ODEs with an ODE solver VODE [20].

Once the time series of ψ' are obtained, a DMD method [16] is employed to extract the eigenvalues α_i for mode i ($i=0, \dots, n$) from the time series of dimensionless form of $\psi' = \psi' / (a_f)_a$, here a_f is the frozen sonic speed. It should be noted in particular that the eigenvalues α_i used hereinafter in the present work are all in dimensionless form that characterizes the perturbation mode in detonation system. α_i is a complex number, where its real part α_{re} represents the growth rate of the perturbation, and its imaginary part α_{im} represents the frequency of the perturbation. Each eigenvalue represents a mode of perturbation, which is sorted by perturbation frequency from low to high as mode 0, mode 1, and so on. If the growth rate of all modes obtained by the DMD is less than 0, the perturbation is decayed, indicating that the detonation wave is stable in this case, otherwise the detonation wave is unstable. The details of computational procedure of the DMD method can be found in the Ref. [16].

To determine the grid resolution in the finite difference approximations, a grid independence test in the computations of the linear stability analysis is carried out, for the case of detonation of stoichiometric H_2/O_2 mixture with 40 vol% Ar dilution ratio at an initial pressure of 1 atm (1 atm = 1.01325×10^5 Pa). Table 1 shows the eigenvalues of the first four perturbation modes at three grid resolutions. It can be found that as the grid number per l_{ind} increases, the real and imaginary parts of the eigenvalue α_i only show the slight changes, indicating that the value of α_i is independent of the grid resolution under the given three grid resolutions. Considering the accuracy and cost of the computational results, the grid resolution of 160 pts/ l_{ind} (pts/ l_{ind} is the number of grid points in the length of each induction zone) is adopted in the subsequent linear stability computations.

3. Nonlinear stability analysis method

To compare with the linear stability computation results, the reactive Euler Eqs. (1)-(4) are directly integrated to a one-dimensionally direct numerical simulation to examine the nonlinear unstable propagation characteristics of detonation waves for $\text{H}_2/\text{O}_2/\text{Ar}$ mixture and the one-dimensionally longitudinal oscillation characteristics of detonation waves. In the solution process, the finite difference method is used to discretize the Eqs. (1)-(4), in which the convection term is solved by the combination of Lax-Friedrichs flux splitting and the fifth-order nonlinear weighted non-oscillatory (WENO) scheme [21]. The implicit ODE solver (VODE) is used to solve the chemical source term that described by the same detailed reaction mechanism as that in Sect. 2. In addition, the third-order Runge-Kutta algorithm is used to approximate the time derivative term in the governing equations. In order to ensure the explicitly time-marching stability of the simulation, the Courant-Friedrichs-Lewy number is set to 0.3.

We design a one-dimensionally computational domain in laboratory coordinate. To observe the long-term behavior of nonlinear stability characteristics of the detonation wave, the length of the computational domain is set to be 1,000 times the induction zone length l_{ind} . For certain special cases, the computational domain is further extended when the detonation wave takes longer to approach to a steady-state solution, in order to ensure the accuracy and reliability of the results.

To determine the appropriate grid resolution, we also

Table 1 The eigenvalues of first four perturbation modes at the different grid resolutions

Grid resolution (pts/ l_{ind})	α_1	α_2	α_3	α_4
80	0.0139+0.6096i	0.0681+4.1709i	-0.3545+7.9009i	-0.8825+11.5557i
160	0.0142+0.6089i	0.0687+4.1712i	-0.3540+7.9007i	-0.8821+11.5556i
320	0.0144+0.6084i	0.0691+4.1712i	-0.3537+7.9006i	-0.8818+11.5555i

carried out the grid independence test of the one-dimensionally nonlinear oscillation process of the detonation wave for the stoichiometric H₂/O₂ mixture diluted by 40% Ar at an initial pressure of 1 atm. Figure 1 shows the time histories of pressure peak of detonation at different grid resolutions. The pressure peak is represented by the value of the leading shock of the detonation wave, normalized by the initial pressure p_0 . It can be seen that the pressure peaks obtained by three different grid resolutions show the periodic oscillation pattern. When the grid resolution is 16 pts/ l_{ind} , the pressure peak has a high amplitude. With the increase of grid resolution, the amplitude of the pressure peak decreases rapidly. It can be seen that the difference between the results of 32 and 64 pts/ l_{ind} is obviously small with each other. The results of Fig. 1 also show that oscillation frequency of the pressure peaks is not much different among these grid resolutions. In order to further quantitatively compare the computational results for different grid resolutions, a fast Fourier transform (FFT) method is adopted to process the results in Fig. 1 to obtain the oscillation period and amplitude of the pressure peak at these grid resolutions, as shown in Table 2. Note that the induction time t_{ind} in the table represents the time that the fluid particle moves within an induction zone length l_{ind} . It can be seen from the results in Table 2 that when the grid resolution increases from 16 to 32 pts/ l_{ind} , the oscillation period T decreases from 11.494 to 10.309 t_{ind} , the amplitude D_p decreased from 21.120 p_0 to 9.627 p_0 . However, when increasing from 32 to 64 pts/ l_{ind} for grid resolution, T and D_p

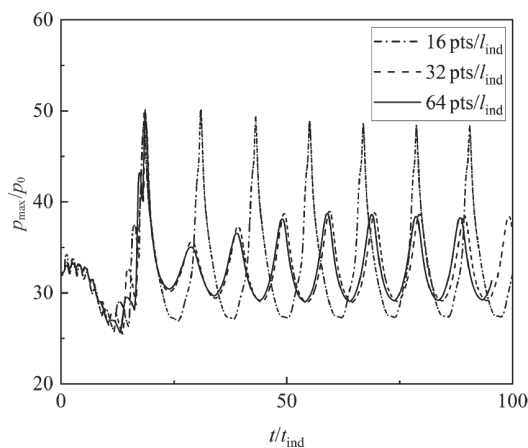


Figure 1 Time histories of pressure peak under the different grid resolutions.

Table 2 The oscillation period (T) and amplitude (D_p) of pressure peak of detonation wave for stoichiometric H₂/O₂ mixture diluted by 40% Ar at different grid resolutions^{a)}

Grid resolutions (pts/ l_{ind})	T (t_{ind})	D_p (p_0)
16	11.494	21.120
32	10.309	9.627
64	10.204	9.340

a) $p_0=1$ atm.

almost did not change. This indicates that rougher grid (such as 16 pts/ l_{ind}) will lead to larger pressure peak amplitude fluctuations, whereas the finer grid can produce smaller amplitude of pressure peak and the convergent results. The results in Table 2 show that 32 pts/ l_{ind} is a reasonable choice, which avoids excessive computational costs while ensuring the accuracy of the simulations. Therefore, a grid resolution of 32 pts/ l_{ind} is selected for the subsequent numerical simulations of present study.

To illustrate the content of this paper more clearly, a schematic diagram on computational methods for both linear and nonlinear stability problems is presented, as shown in Fig. 2.

4. Result and discussion

4.1 Effect of controlling parameters

For the global reaction systems, the activation energy, adiabatic index, reaction heat release and detonation overdrive can usually be regarded as the parameters affecting the stability of gaseous detonation wave propagation [22]. However, for the complex reaction systems, most of the above parameters can neither be easily determined nor have practical significance. In general, the apparent activation energy, the thermal effect and the adiabatic index in complex reaction systems depend on the composition of reactive gases. Therefore, the selection of gas composition as a controlling parameter can not only investigate the stability of detonation, but also is significant in selecting the appropriate gas in industrial safety applications. In addition,

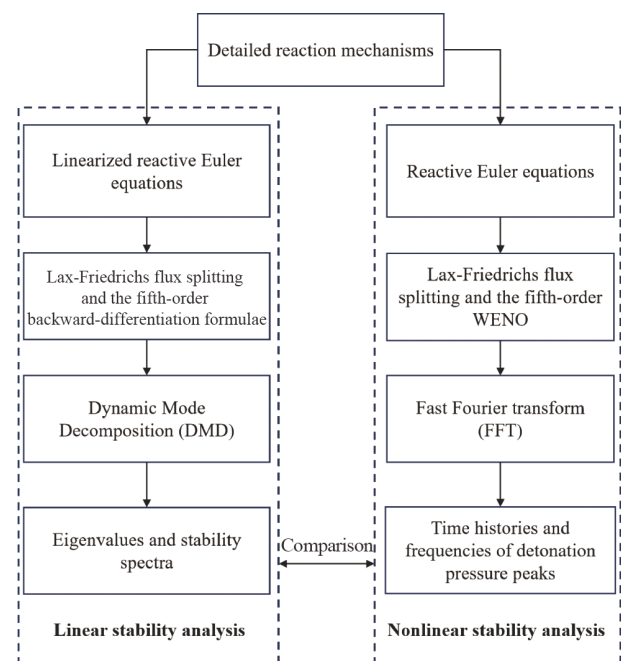


Figure 2 Schematic diagram of computational methods in present study.

environmental conditions (such as initial pressure and temperature) also have a significant effect on the stability of gaseous detonation waves. Therefore, for the $\text{H}_2/\text{O}_2/\text{Ar}$ mixture in the present study, we choose the initial pressure (p_0) and Ar dilution ratio (volume percentage) as the controlling parameters to study their influence on the detonation stability.

In Sect. 2.3, we have shown that the linear stability spectrum is extracted from the time series of $\overline{\psi'}$ by the DMD method. Therefore, before exploring the effects of controlling parameters on the stability spectrum, the time histories of $\overline{\psi'}$ are first analyzed. Figure 3 shows that variations of $\overline{\psi'}$ with time at the two typical initial pressures p_0 of 0.3 and 0.8 atm, respectively, for stoichiometric H_2/O_2 mixture diluted by 30% Ar. Figure 3a shows a stable detonation case, in which the speed perturbation of the propagating detonation wave shows a two-mode oscillation pattern: A low frequency mode superposed by a high frequency mode. A dashed curve is plotted as an envelope curve of the speed perturbation pattern. Obviously, the low frequency perturbation exhibits the exponential decay ($\sim e^{-0.089t/t_{\text{ind}}}$), indicating that the detonation process is immune to external infinitesimal perturbations, especially for the low-frequency component. Such results also suggest that the real part α_{re} of the eigenvalues extracted from time series of ψ' is equal to the coefficient on the exponential term of the envelope curve, at which the coefficient (-0.089) is negative in this case. On the contrary, the envelope curve for speed perturbation pattern in the case with elevated initial pressure ($p_0=0.8$ atm), as shown in Fig. 3b, shows the unstable detonations, in which the perturbation exponentially grows with a positive coefficient on the exponential term of the envelope curve (0.177). The result in Fig. 3b indicates that the detonation process cannot resist external infinitesimal perturbations and gradually becomes unstable when initial pressure rises.

Given the time series of speed perturbation of detonation, we can determine the growth rate and the frequency of all perturbation modes at the specified controlling parameters of detonation. Figure 4 gives the stability spectra of detonation at several typical initial pressures p_0 for the stoichiometric H_2/O_2 mixture with 30% Ar dilution ratio. Here the stability spectra are exhibited by perturbation modes with corresponding complex α_i , in which the horizontal axis α_{re} represents the real part of α_i corresponded to the perturbation growth rate, while the vertical axis α_{im} represents the imaginary part of α_i corresponded to the perturbation frequency. For each initial pressure, the symbols in the figure represent several modes of linear stability of detonation. The mode with the smallest perturbation frequency is defined as mode 0. With the increase of the perturbation frequency, the corresponding modes can be sequentially

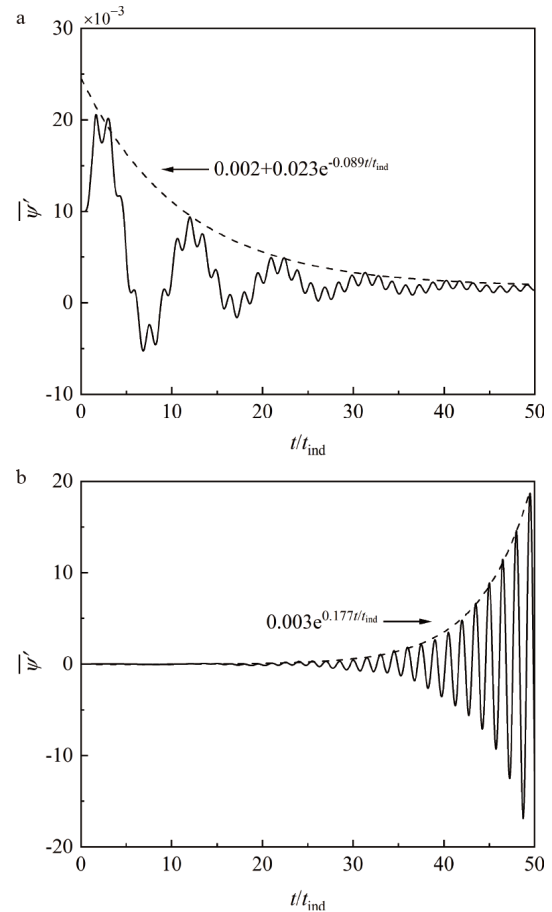


Figure 3 Time series of speed perturbation of detonation for stoichiometric H_2/O_2 with 30% Ar dilution ratio at different initial pressures. **a** $p_0=0.3$ atm; **b** $p_0=0.8$ atm.

referred to as mode 1, mode 2, etc. It can be seen from Fig. 4 that there are two unstable modes (mode 0 and mode 1) in the case of $p_0=0.8$ atm, at which they are located on the right of the vertical dashed line in Fig. 4 ($\alpha_{\text{re}} > 0$). The perturbation growth rate (α_{re}) and the perturbation frequency (α_{im}) of mode 0 are 5.846×10^{-2} and 0.591, respectively, while the α_{re} and α_{im} of mode 1 are 0.177 and 4.195, respectively. Note that the value of α_{re} for mode 1 is just the coefficient on the exponential term of the envelope in Fig. 3b for the same case. When the initial pressure is reduced to $p_0=0.6$ atm, the α_{re} of mode 0 decreases from 5.846×10^{-2} at 0.8 atm to 8.881×10^{-3} , and the α_{re} of mode 1 decreases from 0.177 to 0.109, indicating that unstable detonation is diminished with decreasing initial pressure. When the initial pressure is reduced to 0.4 atm, only mode 1 remains unstable, with its growth rate further decreasing to 1.819×10^{-2} , suggesting a further reduction in instability. When the initial pressure is further reduced ($p_0=0.2$ atm), the unstable mode will no longer appear in the stability spectra and the propagation of detonation wave is linearly stable. In addition, it is also found from the results in Fig. 4 that the perturbation frequency for each mode remains basically unchanged when

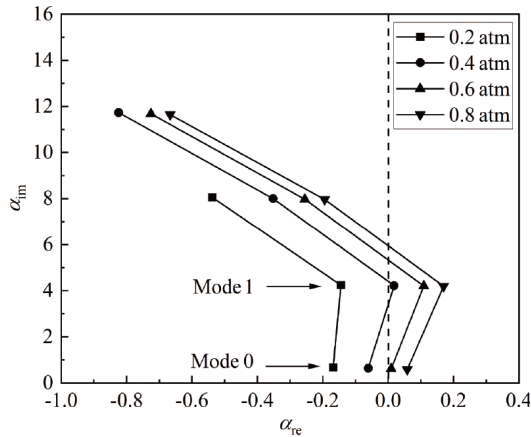


Figure 4 The stability spectra of stoichiometric H_2/O_2 with 30% Ar dilution ratio at different initial pressures.

the initial pressure is changed.

The results of Fig. 4 show that for 30% Ar diluted H_2/O_2 mixture, the decrease of initial pressure is beneficial to stabilizing the detonation. To compare with the nonlinear stability results of detonation wave under the same parameter conditions, we numerically simulate the one-dimensionally nonlinear oscillation characteristics of detonation wave under four initial pressures of 0.2, 0.4, 0.6 and 0.8 atm for the same mixture, as shown in Fig. 5. In the figure, the nonlinear oscillation of the detonation wave is characterized by recording the pressure peak time history of

the leading shock front of detonation wave. The results in Fig. 5a show that when the initial pressure is low ($p_0=0.2$ atm), the pressure peak quickly tends to be constant after an initial large oscillation, indicating that the propagation of the detonation wave under this p_0 is nonlinearly stable, which is consistent with the results of linear stability computed under the same parameter conditions in Fig. 4. In Fig. 5b ($p_0=0.4$ atm), the pressure peak of the detonation wave firstly shows the pattern of low-frequency, low-amplitude oscillation after experiencing the initial large-amplitude oscillation, and then gradually transforms into an oscillation mode superposed by high-frequency and low-frequency perturbations. The amplitude of the superposed mode decreases slowly with time. The high-frequency, low-amplitude component in this oscillation mode represents a critical state of detonation instability, which will be discussed further in the next section. With the further increase of the initial pressure, the pressure peak time history of the detonation wave finally presents a single oscillation mode. For the case of $p_0=0.6$ atm, the amplitude of the single oscillation is about $12 p_0$ (Fig. 5c), while for the case of $p_0=0.8$ atm, the amplitude of the oscillation increases to about $17 p_0$, indicating that with the increase of the initial pressure, the pressure peak of the detonation wave becomes more unstable.

Comparing the results in Fig. 4 with those in Fig. 5, it can be found that the results from linear stability analysis are

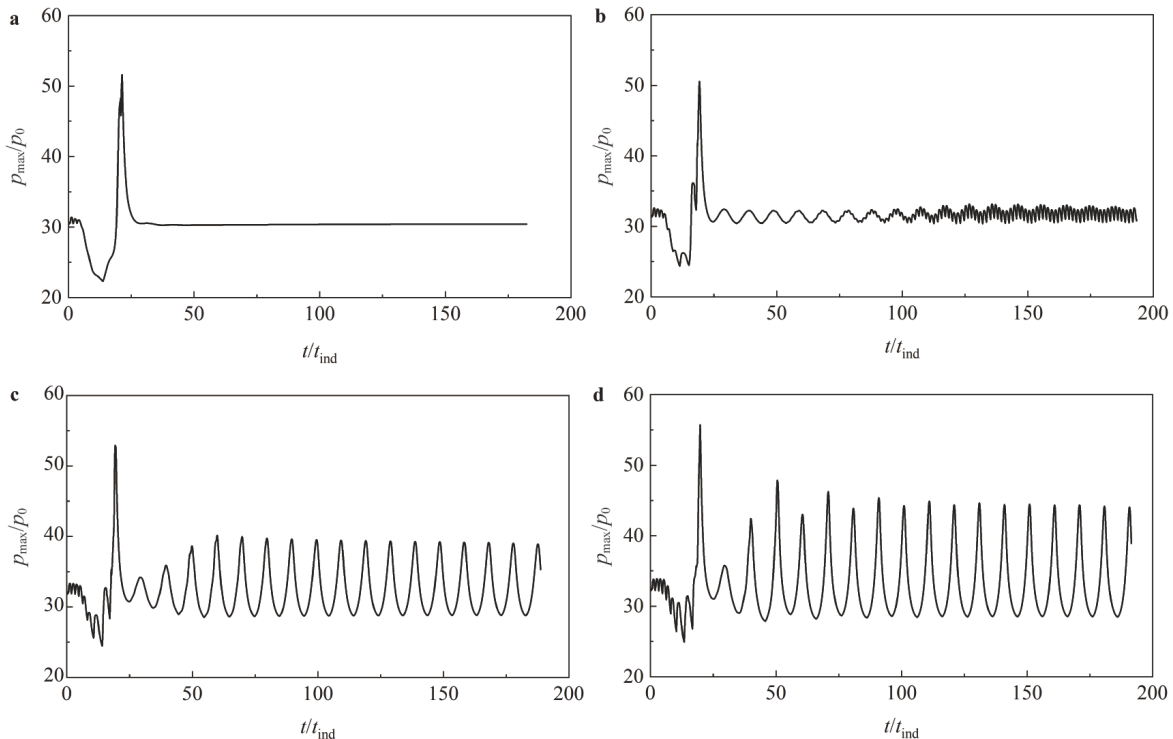


Figure 5 Time histories of pressure peak of detonation for stoichiometric H_2/O_2 mixture with 30% Ar dilution ratio at different initial pressures. **a** $p_0=0.2$ atm; **b** $p_0=0.4$ atm; **c** $p_0=0.6$ atm; **d** $p_0=0.8$ atm.

consistent with those from nonlinear stability simulations. In Fig. 4, the linear stability results indicate that at $p_0=0.4$ atm, there exists only one unstable mode (mode 1) with a relatively small perturbation growth rate ($\alpha_{re}=1.819 \times 10^{-2}$), suggesting that the propagation of the detonation wave is approaching a stable state at this initial pressure. Furthermore, the results in Fig. 5b demonstrate that under the same initial pressure, the time history of pressure peak of the detonation wave reaches a critical state characterized by high-frequency, low-amplitude fluctuations, which qualitatively aligns with the findings from the linear stability analysis. As the initial pressure increases, both linear and nonlinear results indicate that the instability of the detonation wave gradually intensifies.

To investigate the impact of Ar dilution ratio on the stability of detonation, Fig. 6 illustrates the linear stability results of the detonation at various Ar dilution ratios and a fixed initial pressure of $p_0=1$ atm. The results show that at the 20% Ar dilution ratio, there are three unstable modes (mode 0, mode 1, and mode 2), with the most unstable mode 1 exhibiting a perturbation growth rate of 0.364. As the Ar dilution ratio increases, the perturbation growth rate of the most unstable mode 1 gradually decreases, indicating that higher Ar dilution ratio leads to more stable detonation wave. Additionally, the results in Fig. 6 reveal that modes with higher perturbation frequencies experience a more rapid decline in growth rate with an increasing Ar dilution ratio. However, the change of Ar dilution ratio does not significantly alter the perturbation frequencies of the same modes, suggesting that within a certain range, the periodicity of the perturbation remains relatively constant. This conclusion is consistent with the experimental results of Mcvey and Toong [23] and Lee's linear stability analysis [5].

Figure 7 presents the results of the one-dimensionally nonlinear oscillation of the detonation wave under the same parameter conditions as in Fig. 6. Figure 7a is the pattern of pressure peak at 20% Ar dilution ratio. One can see that

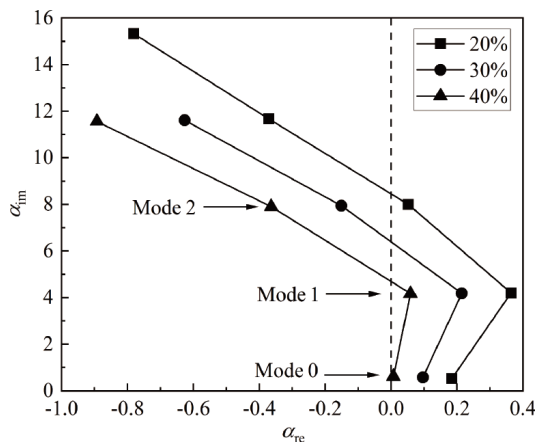


Figure 6 The stability spectra of stoichiometric H_2/O_2 at the different Ar dilution ratios, $p_0=1$ atm.

under this Ar dilution ratio, the pressure peak shows a trend of increasing amplitude with time after experiencing a series of irregular oscillations. The raised amplitude makes the pressure at the trough position of oscillation pattern continue to decrease, so that detonation may be extinguished due to the excessive attenuation of shock wave intensity in the later stage, indicating that the detonation is extremely unstable in this case. When the Ar dilution ratio increases to 30%, the time history of pressure peak eventually exhibits the characteristics of dual-mode oscillation with low-frequency, high-amplitude pattern, as shown in Fig. 7b. Although this oscillation is still unstable, it is weaker than that in the case with 20% Ar dilution ratio. When the Ar dilution ratio is further increased to 40%, the pressure peak is finally presented as a single-mode oscillation with a low-frequency, medium-amplitude pattern. The above results clearly show that with the increase of Ar dilution ratio, the detonation of $H_2/O_2/Ar$ mixture is gradually stable, which is qualitatively consistent with the results by linear stability analysis in Fig. 6.

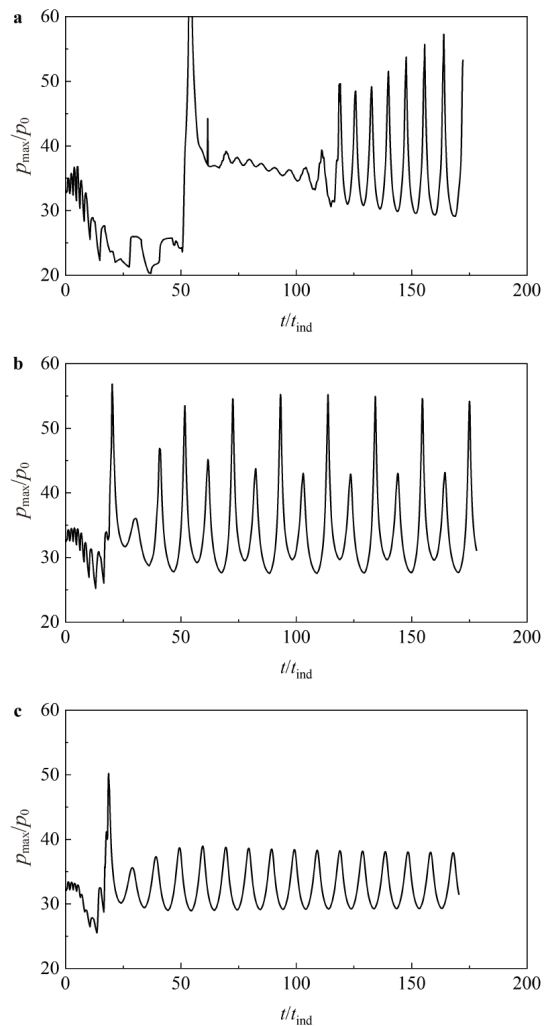


Figure 7 Time histories of pressure peak of detonation for stoichiometric H_2/O_2 mixture at different Ar dilution ratios, $p_0=1$ atm. **a** 20% Ar; **b** 30% Ar; **c** 40% Ar.

4.2 Critical stability curves

Both the results from linear stability computations and one-dimensionally nonlinear numerical simulations in previous section demonstrate that the initial pressure and the Ar dilution ratio in the complex reaction system significantly influence the stability of detonation waves in $\text{H}_2/\text{O}_2/\text{Ar}$ mixture. To further quantitatively compare the results obtained from the two methods, we plot the critical stability curves for mode 0 and mode 1 on the phase plane of p_0 -Ar% based on the results from linear stability analysis. The selected range for p_0 is from 0 to 1.4 atm, while the Ar dilution ratio ranges from 0 to 45%. To determine the stability boundaries for a given mode, we first specify an Ar dilution ratio and then identify the critical value of p_0 at which the growth rate of that mode approaches to zero, allowing for a relative error of 10^{-3} .

Figure 8 presents two critical stability curves for mode 0 and mode 1 in the p_0 -Ar% plane, determined by using the linear stability method. It is evident that the stability curve for mode 1 does not intersect with the curve for mode 0 within the given p_0 -Ar% plane, with the stability curve for mode 1 located below that for mode 0. Linear stability results indicate that only below the stability curve for mode 1 do all modes exhibit a negative growth rate, meaning that in the p_0 -Ar% plane, the stability of the detonation wave is governed by the critical stability curve of mode 1. Therefore, we call this curve the neutral stability curve of mode 1. On the other hand, linear stability results also show that the perturbations above the critical stability curve of mode 0 exhibit the positive growth rate for low-frequency mode 0, while the perturbations below the curve of mode 0 but above the curve of mode 1 display the negative growth rate for low-frequency mode 0 and the positive growth rate for high-frequency mode.

This suggests that the critical stability curve of mode 0 separates the high-frequency perturbation mode from the low-frequency perturbation mode. Thus, we can also call the critical stability curve of mode 0 the perturbation frequency transition curve. For analytical convenience, we define the stable region below the neutral curve of mode 1 as region I. Above the neutral curve of mode 1, the frequency transition curve of mode 0 further divides this unstable area into two regions: The area above the curve of mode 0 is defined as region III, while the area between both curves of modes 0 and 1 is defined as region II. Clearly, region III represents a linearly unstable area, while region II serves as a transitional area situated between the stable region I and the unstable region III.

To further compare with the nonlinear oscillation behavior of detonation, we selected several suitable parameter pairs (p_0 , Ar%) within the p_0 -Ar% plane shown in Fig. 8 and conducted numerical simulations of one-dimensionally

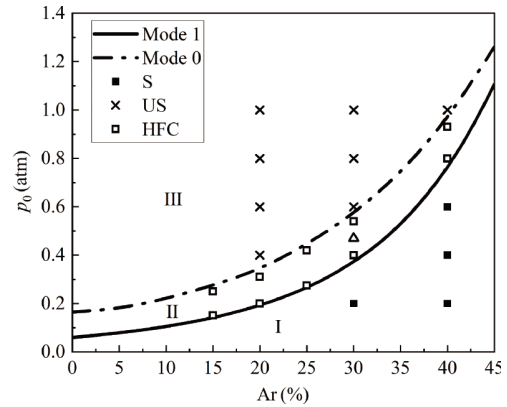


Figure 8 Critical stability curves determined by linear stability analysis for mode 0 and mode 1, symbols are the result determined by nonlinear numerical simulations. S - stable, US - unstable, HFC - high frequency critical.

nonlinear oscillatory detonation. The numerical results show that all cases exhibiting pressure oscillation over time (marked as “x” and “□”) are located above the neutral stability curve of mode 1, while all cases in which the pressure oscillations ultimately decay (marked as “■”) fall below this curve. These results suggest that in complex reactive systems considering detailed elementary chemical mechanisms, the results of linear stability computations well agree with those of one-dimensionally nonlinear oscillation of pressure peak of detonation wave. Ng et al. [24] found that the critical activation energy for one-dimensionally non-linear instability of detonations obtained from numerical simulations of a single-step reaction corresponds well with the linear stability results under the same conditions. Weng and Mével [9] studied the linear stability and one-dimensionally nonlinear stability results using a single-step chemical reaction model that accounts for molecular volume effects, and the good agreement between the linear and nonlinear results was obtained. Sharpe and Falle [25] addressed the stability of pathological detonations in a two-step consecutive reaction model consisting of an exothermic reaction followed by an endothermic reaction, identifying strong correlations between linear stability theory and nonlinear oscillation characteristics. In the present study, the results from Fig. 8 also suggest that the linear stability analysis results for complex reaction systems are consistent with those from one-dimensionally nonlinear numerical simulations.

4.3 Stability analysis of frequency transition region

In Fig. 8, region II between the curves of mode 0 and mode 1 is particularly interesting. The parameters selected for the one-dimensionally nonlinear oscillation case shown in Fig. 5b are located in this region. From the results of Fig. 5b, the peak pressure of the detonation wave shows a significant

high-frequency characteristic, which is very different from the low-frequency instability in region III (such as cases in Fig. 5c and d). To explore the nonlinear oscillation characteristics of detonation wave in this region, we select five Ar ratios of 15%, 20%, 25%, 30%, and 40% as the Ar dilution parameters. For each Ar dilution ratio, we also select a high initial pressure near the curve of mode 0 and a low initial pressure near the curve of mode 1 as the p_0 parameter, respectively. Such selections produce 10 computational cases that are marked with “□” in region II of Fig. 8.

Figure 9 presents the numerical simulation results for five cases near the lower boundary (the neutral stability curve of mode 1) in region II. When the Ar dilution ratio is 15%, the pattern of pressure peak over time exhibits a clear high-frequency, low-amplitude oscillation pattern (Fig. 9a) after several large initial oscillations and subsequent decay. At 20% and 25% of Ar dilution ratios, the pressure peak first exhibits the significant initial oscillations. These oscillations subsequently transform into a low-frequency, low-amplitude pattern. Ultimately, they shift back to a high-frequency, low-amplitude mode (Fig. 9b and c). As the Ar dilution ratio increases to 30%, the decay of the low-frequency, low-amplitude mode slows down but the growth of the high-frequency, low-amplitude mode becomes more pronounced. Thus, a superposed oscillation mode with low and high frequencies is shown in late stages of time history of pressure peak, as shown in (Fig. 9d). When the Ar dilution ratio is further increased to 40%, the long-term behavior of the pressure peak exhibits a unique oscillation pattern in which the high-frequency perturbation is overlaid by the low-frequency perturbation (Fig. 9e). A locally enlarged pattern of

oscillation mode in Fig. 9e is shown in Fig. 9f, the enlarged figure clearly illustrates the pattern from the superposition of these two oscillation modes, which is similar to Fig. 7 in one-dimensional pulsating detonation of two-step chain-branch reaction model by Leung et al. [26]. These results indicate that within the selected range of Ar dilution ratio in present study, region II displays high-frequency, low-amplitude oscillation characteristics near the low boundary of stability. This implies that the results from the linear stability analysis also contain components of high-frequency perturbations near the low boundary of region II. Furthermore, it is found that as Ar dilution ratio increases, the amplitude of high-frequency oscillations gradually decreases, and the transition of pressure peak from low-frequency mode to high-frequency mode requires a longer time. This is attributed to the decreasing difference in growth rates between high-frequency and low-frequency modes when Ar dilution ratio rises (see Fig. 6), leading to a longer period for their growth or decay.

In addition to examining the stability characteristics of detonation near the lower boundary of region II, we also investigate the properties of one-dimensionally nonlinear oscillations near the upper boundary (the perturbation frequency transition curve of mode 0) within this region. Figure 10 shows the time histories of pressure peak of detonation wave under five different Ar dilution ratios near the upper boundary of region II. At Ar dilution ratios of 15% and 20%, the pressure peaks experience significant initial oscillations and then form a superposed pattern of high-frequency and low-frequency perturbations. Over time, this pattern gradually evolves into a low-frequency, high-amplitude oscillation mode (Fig. 10a and b). However, when

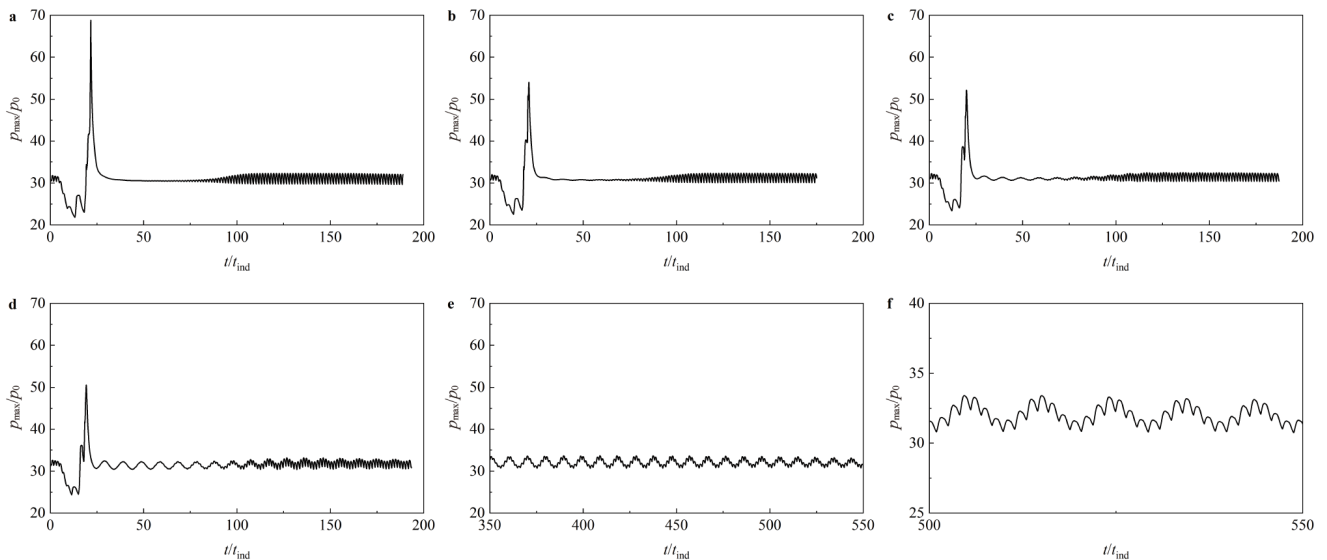


Figure 9 Time histories of pressure peak of detonation for different cases near the lower boundary (the curve of mode 1) of region II. **a** $p_0=0.15$ atm, 15% Ar; **b** $p_0=0.20$ atm, 20% Ar; **c** $p_0=0.275$ atm, 25% Ar; **d** $p_0=0.40$ atm, 30% Ar; **e** $p_0=0.80$ atm, 40% Ar; **f** locally enlarged subset of **e**.

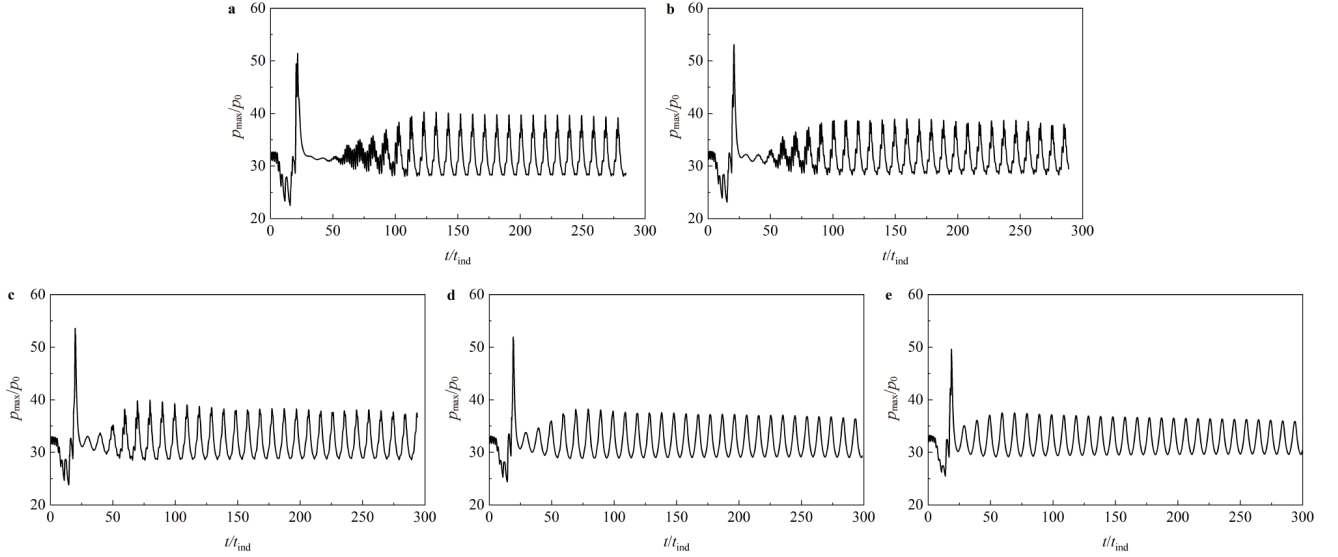


Figure 10 Time histories of pressure peak of detonations for different cases near the upper boundary (the curve of mode 0) of region II. **a** $p_0=0.25$ atm, 15% Ar; **b** $p_0=0.31$ atm, 20% Ar; **c** $p_0=0.42$ atm, 25% Ar; **d** $p_0=0.54$ atm, 30% Ar; **e** $p_0=0.93$ atm, 40% Ar.

the Ar dilution ratio increases to 25% or higher (Fig. 10c-e), the initial high-frequency perturbations become less pronounced, and the pressure peaks primarily exhibit low-frequency, high-amplitude oscillation behavior over time.

The results in Fig. 10 also reveal that in all cases, the pressure peaks characterized by low-frequency, high-amplitude pattern gradually decay over time. Especially, this decay becomes more pronounced at higher Ar dilution ratios (as seen in Fig. 10e). At lower Ar dilution ratios, the decay of pressure peaks is weaker, with even slightly initial growth observed (as shown in Fig. 10c). To further investigate these oscillatory behaviors of pressure peak, we perform a fast Fourier transformation on the time series of pressure peaks for the five cases in Fig. 10. From the transformed results, we extract the perturbation frequencies with significant oscillation amplitudes, denoted as f_{num} . Additionally, we also analyze the perturbation growth rates α_{re} and perturbation frequencies α_{im} for modes 0 and 1 obtained from the linear stability results of these five cases. These results are summarized in Table 3. Note that the linear perturbation frequencies α_{im} and the nonlinear perturbation frequencies f_{num} in the table are comparable, and their differences can be expressed by using the following relative error ε

$$\varepsilon = \frac{|f_{\text{num}} - \alpha_{\text{im}}|}{\alpha_{\text{im}}} \times 100\%, \quad (25)$$

where the value of ε represents the difference of perturbation frequencies between the linear and nonlinear results.

The results in Table 3 show that the results of the five cases at the locations near the perturbation frequency transition curve of mode 0 in region II are similar to each other. Therefore, the results of the case 3 with Ar dilution ratio of 25% are taken as an example to illustrate. In this case, the

Table 3 Comparisons between the linear stability computations and the FFT results from nonlinear numerical simulations for cases near the upper boundary of region II

Case	Ar (%)	p_0 (atm)	Mode	$\alpha_{\text{re}} (10^{-2})$	$\alpha_{\text{im}} (1/t_{\text{ind}})$	$f_{\text{num}} (1/t_{\text{ind}})$	ε (%)
1	15	0.25	0	-1.740	0.624	0.631	1.12
			1	13.847	4.239	3.884	8.37
2	20	0.31	0	-2.036	0.624	0.637	2.08
			1	11.453	4.237	3.809	10.1
3	25	0.42	0	-0.948	0.620	0.634	2.26
			1	10.752	4.221	3.804	9.88
4	30	0.54	0	-0.923	0.618	0.637	3.07
			1	8.568	4.206	3.754	10.7
5	40	0.93	0	-0.547	0.615	0.638	3.74
			1	4.337	4.173	3.878	7.07

linear stability analysis shows that the perturbation growth rate of mode 0 ($\alpha_{\text{re}} = -9.48 \times 10^{-3}$) is negative, and its perturbation frequency is small ($\alpha_{\text{im}}=0.620$), indicating that mode 0 is a decaying low-frequency perturbation. The perturbation growth rate of mode 1 ($\alpha_{\text{re}}=0.10752$) is positive, and its perturbation frequency is large ($\alpha_{\text{im}}=4.221$), indicating that mode 1 is a growing high-frequency perturbation. On the other hand, the nonlinear numerical simulation for the same case also produces two perturbation modes. The frequency of the low-frequency perturbation mode is in good agreement with the result of the low-frequency perturbation of linear stability ($\varepsilon=2.26\%$), while the high-frequency perturbation result is also in reasonable agreement with the high-frequency perturbation result of linear stability ($\varepsilon=9.88\%$). Weng and Mével [9] also compared the perturbation frequencies between the linear and nonlinear results in the detonation stability analysis with single-step reaction considering molecular effect. The range of relative error (ε) of their results is between 0.038% and 5.0% by using the

same Eq. (25). This error range is consistent with the error range of the low-frequency perturbations we predicted (1.12-3.74%) and is on the same order of magnitude as that of the high-frequency perturbations we obtained (7.07-10.07%), which can demonstrate the validity of our calculations.

The results of Table 3 demonstrate that oscillation pattern of the pressure peak in Fig. 10 still contains high-frequency perturbation component, and the oscillation pattern is the result of the superposition between high-frequency perturbation and low-frequency perturbation. From the five cases in Table 3, it can be further observed that as Ar dilution ratio increases, both the decay rate of mode 0 and the growth rate of mode 1 show a slower trend. Therefore, the pattern of pressure peak obtained by nonlinear simulations in Fig. 10 is related to the growth and decay of the amplitude of the two modes. For case 1, although the low-frequency, high-amplitude perturbation decays ($\alpha_{re} = -0.0174$), the superimposed perturbation decays slowly, due to the rapid growth of high-frequency, low-amplitude perturbation ($\alpha_{re} = 0.13847$) (see Fig. 10a). For case 5, due to the slow growth of high-frequency, low-amplitude perturbation ($\alpha_{re} = 0.04337$), the decay of the superposed perturbation becomes more obvious (see Fig. 10e). For case 3, with moderate growth of high-frequency perturbations and the relatively moderate decay of low-frequency perturbations, the overall pressure peak first increases to the maximum value and then gradually decays (see Fig. 10c).

Although the results in Table 3 show that the low-frequency perturbation of mode 0 of these five cases decays, their decay is very slow because these cases are located near the frequency transition curve of mode 0. In the numerical simulation of the longitudinal oscillation of the pressure peak in Fig. 10, the complete decay of the low-frequency oscillation would take a very long time (Fig. 10 does not show this). However, it can be expected that the high-frequency oscillation will eventually appear, if decay time of the low-frequency oscillation is long enough. The above analysis confirms that the curve of mode 0 is the critical curve separating the low-frequency perturbations from the high-frequency perturbations. This conclusion is consistent with the results obtained by Short and Wang [27] using the three-step chain branching reaction model.

Figures 9 and 10 show the difference in longitudinal nonlinear oscillation of the pressure peak of detonation wave between near the lower boundary of region II (the neutral curve of mode 1) and near the upper boundary of region II (the perturbation frequency transition curve of mode 0). For these cases, the former shows a primary high-frequency, low-amplitude oscillation mode, while the latter mainly shows a low-frequency, high-amplitude oscillation mode. To further illustrate the continuous transition from the high-frequency mode to the low-frequency mode in the re-

gion, we also add a case with an initial pressure $p_0 = 0.47$ atm and a 30% Ar dilution ratio, which is located in the middle of the region II (see the case marked as “ Δ ” in Fig. 8). Figure 11 shows the time history of pressure peak and its locally enlarged results for this case. This result clearly demonstrates the interaction between high-frequency and low-frequency perturbations, which is similar to that in Fig. 9f. Both results in Figs. 11b and 9f suggest a continue transition of perturbation from low-frequency, high-amplitude oscillation to high-frequency, low-amplitude oscillation in region II, when initial pressure gradually decreases or Ar dilution ratio gradually increases. These results obtained by numerical simulations verify the accuracy and effectiveness of the linear stability theory in predicting the stability of detonation waves in complex chemical reaction systems. By virtue of the low-cost characteristic of linear stability calculations, it can greatly save resources when predicting the stability of detonation waves and selecting appropriate initial conditions for detonation stability research in complex reactive systems. However, our predictions can only cover the one-dimensional perturbation case, and more research is still needed for linear stability analysis on multi-dimensional perturbations in complex reactive systems.

5. Conclusion

In present study, a finite difference numerical method and DMD perturbation analysis are combined to perform the

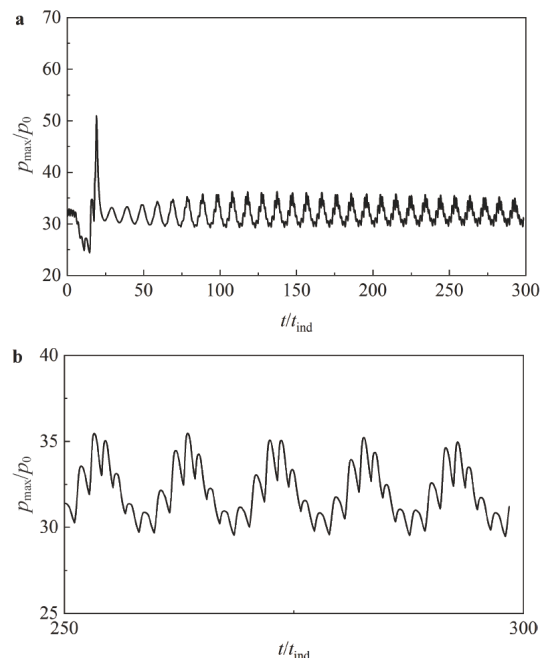


Figure 11 Time histories of pressure peak of detonation for case with $p_0 = 0.47$ atm and Ar dilution ratio of 30%. **a** Integrated plot; **b** locally enlarged subset.

linear stability analysis of gaseous detonation, based on the detailed chemical reaction mechanism of $\text{H}_2/\text{O}_2/\text{Ar}$. In addition, the high-resolution one-dimensionally direct numerical simulation of detonation wave propagation is carried out to obtain the nonlinear oscillation characteristics of detonation wave for the same $\text{H}_2/\text{O}_2/\text{Ar}$ mixture. The results of linear and nonlinear stabilities are compared and analyzed. The main conclusions are as follows:

(1) The results of linear stability analysis show that for detonation of $\text{H}_2/\text{O}_2/\text{Ar}$ mixture, there are perturbation modes with different frequencies, and all of these perturbation modes can decay with the decrease of initial pressure or the increase of Ar dilution ratio. Whether the initial pressure or the Ar dilution ratio is changed, the dimensionless frequency of the given perturbation mode obtained by the linear stability analysis does not vary. The results of one-dimensionally nonlinear oscillation characteristics of detonation are consistent with those obtained by above linear stability analysis.

(2) Based on the linear stability analysis, two critical stability curves of perturbation modes 0 and 1 are obtained in the p_0 -Ar% phase plane. The neutral stability curve of mode 1 serves as the boundary between stable and unstable regions, while the perturbation frequency transition curve of mode 0 delineates the boundary between high-frequency and low-frequency perturbations within the unstable region. Thus, these two curves divide the entire p_0 -Ar% plane into stable (region I), high-frequency unstable (region II) and low-frequency unstable (region III) regions. The results of one-dimensional nonlinear numerical simulations are consistent with the linear stability results for each region.

(3) In the high-frequency unstable region (region II), the perturbation is the superposition between the low-frequency, high-amplitude mode and the high-frequency, low-amplitude mode. With the decrease of initial pressure or the increase of Ar dilution ratio, the perturbation gradually transits from the low-frequency, high-amplitude mode to the high-frequency, low-amplitude one. The linear stability analysis shows that the frequencies of both perturbation modes are quantitatively consistent with those by the Fourier transform in nonlinear numerical simulation. This consistency indicates that the results of linear stability analysis can well predict the one-dimensionally nonlinear oscillation characteristics of pressure peak of detonation wave in complex reactive systems.

Conflict of interest On behalf of all authors, the corresponding author states that there is no conflict of interest.

Author contributions Junhui Zhang: Formal analysis, Investigation, Writing – original draft. Gang Dong: Conceptualization, Formal analysis, Writing – review & editing.

Acknowledgements The work was supported by the National Natural Science Foundation of China (Grant No. 12472335).

- 1 J. E. Shepherd, Detonation in gases, *Proc. Combust. Inst.* **32**, 83 (2009).
- 2 B. A. Rankin, M. L. Fotia, A. G. Naples, C. A. Stevens, J. L. Hoke, T. A. Kaemming, S. W. Theuerkauf, and F. R. Schauer, Overview of performance, application, and analysis of rotating detonation engine technologies, *J. Propuls. Power* **33**, 131 (2017).
- 3 J. J. Erpenbeck, Stability of steady-state equilibrium detonations, *Phys. Fluids* **5**, 604 (1962).
- 4 J. J. Erpenbeck, Stability of idealized one-reaction detonations, *Phys. Fluids* **7**, 684 (1964).
- 5 H. I. Lee, and D. S. Stewart, Calculation of linear detonation instability: One-dimensional instability of plane detonation, *J. Fluid Mech.* **216**, 103 (1990).
- 6 G. J. Sharpe, Linear stability of pathological detonations, *J. Fluid Mech.* **401**, 311 (1999).
- 7 A. Mégevand, and F. A. Membiela, Stability of cosmological detonation fronts, *Phys. Rev. D* **89**, 103503 (2014).
- 8 K. C. K. Uy, L. Shi, J. Hao, and C. Y. Wen, Linear stability analysis of one-dimensional detonation coupled with vibrational relaxation, *Phys. Fluids* **32**, 126101 (2020).
- 9 Z. Weng, and R. Mével, Linear and non-linear stability of gaseous detonation at elevated pressure, *Combust. Flame* **262**, 113361 (2024).
- 10 G. J. Sharpe, Linear stability of idealized detonations, *Proc. R. Soc. Lond. A* **453**, 2603 (1997).
- 11 M. Short, and J. W. Dold, Linear stability of a detonation wave with a model three-step chain-branching reaction, *Math. Comput. Model.* **24**, 115 (1996).
- 12 Z. Liang, and L. Bauwens, Detonation structure with pressure-dependent chain-branching kinetics, *Proc. Combust. Institute* **30**, 1879 (2005).
- 13 S. T. Kao, Detonation Stability with Reversible Kinetics, Dissertation for the Doctoral Degree (California Institute of Technology, Pasadena, 2008).
- 14 D. I. Kabanov, and A. R. Kasimov, Linear stability analysis of detonations via numerical computation and dynamic mode decomposition, *Phys. Fluids* **30**, 036103 (2018).
- 15 M. P. Burke, M. Chaos, Y. Ju, F. L. Dryer, and S. J. Klippenstein, Comprehensive H_2/O_2 kinetic model for high-pressure combustion, *Int. J. Chem. Kinetics* **44**, 444 (2012).
- 16 P. J. Schmid, Dynamic mode decomposition of numerical and experimental data, *J. Fluid Mech.* **656**, 5 (2010).
- 17 B. D. Taylor, A. R. Kasimov, and D. S. Stewart, Mode selection in weakly unstable two-dimensional detonations, *Combust. Theor. Model.* **13**, 973 (2009).
- 18 California Institute for Technology, Cantera: Object-Oriented Software for Reacting Flows. <http://www.cantera.org>, 2005.
- 19 J. Lawson, and J. Shepherd, Shock and detonation toolbox installation instructions (California Institute of Technology, Pasadena, 2019).
- 20 P. N. Brown, G. D. Byrne, and A. C. Hindmarsh, VODE: A variable-coefficient ODE solver, *SIAM J. Sci. Stat. Comput.* **10**, 1038 (1989).
- 21 J. Shi, Y. T. Zhang, and C. W. Shu, Resolution of high order WENO schemes for complicated flow structures, *J. Comput. Phys.* **186**, 690 (2003).
- 22 M. Short, and D. S. Stewart, Cellular detonation stability. Part 1. A normal-mode linear analysis, *J. Fluid Mech.* **368**, 229 (1998).
- 23 J. B. Mcvey, and T. Y. Toong, Mechanism of instabilities of exothermic hypersonic blunt-body flows, *Combust. Sci. Tech.* **3**, 63 (1971).
- 24 H. Ng, A. Higgins, C. Kiyanda, M. Radulescu, J. Lee, K. Bates, and N. Nikiforakis, Nonlinear dynamics and chaos analysis of one-dimensional pulsating detonations, *Combust. Theor. Model.* **9**, 159 (2005).
- 25 G. J. Sharpe, and S. A. E. G. Falle, One-dimensional nonlinear stability of pathological detonations, *J. Fluid Mech.* **414**, 339 (2000).
- 26 C. Leung, M. I. Radulescu, and G. J. Sharpe, Characteristics analysis

of the one-dimensional pulsating dynamics of chain-branching detonations, *Phys. Fluids* **22**, 126101 (2010).

27 M. Short, and D. Wang, On the dynamics of pulsating detonations, *Combust. Theor. Model.* **5**, 343 (2001).

复杂反应体系中气相爆轰波的线性和非线性稳定性分析

张俊辉, 董刚

摘要 气相爆轰波的稳定性在基于爆轰推进的超燃动力装置工作过程和工业爆炸灾害过程中起到了重要作用, 然而针对由实际燃料与氧化剂构成, 且需用大量基元反应来描述的复杂反应体系中爆轰波稳定性的研究, 目前还不够深入全面. 为了探究复杂反应体系中气相爆轰波传播的线性和非线性稳定性之间的联系, 本文基于带 $H_2/O_2/Ar$ 详细反应机理的欧拉方程组, 通过线性稳定性分析和一维非线性数值模拟的方法对一维 $H_2/O_2/Ar$ 爆轰过程的稳定性开展了研究. 结果表明, 对于用基元化学反应表达的复杂反应体系, 线性稳定性计算结果与一维非线性纵向振荡爆轰的结果符合得很好. 根据线性稳定性计算结果, 得到了初始压力-惰性气体(氩气)浓度平面的中性稳定性曲线和一条新的低频-高频模式转换的临界曲线. 一维非线性计算结果表明, 在模式转换的临界曲线附近, 爆轰波的振荡会由低频高幅模式转变为高频低幅的模式, 其振荡频率与线性稳定性分析得到的有最大扰动增长率的模态的频率相同. 基于真实预混反应气体的爆轰稳定性研究为实际应用中选择合适的初始条件和气体配比提供了直接的依据.